Article

Silica#Void#Gold Nanoparticles: Temporally Stable Surface-Enhanced Raman Scattering Substrates

Maryuri Roca, and Amanda J. Haes

J. Am. Chem. Soc., **2008**, 130 (43), 14273-14279 • DOI: 10.1021/ja8059039 • Publication Date (Web): 03 October 2008

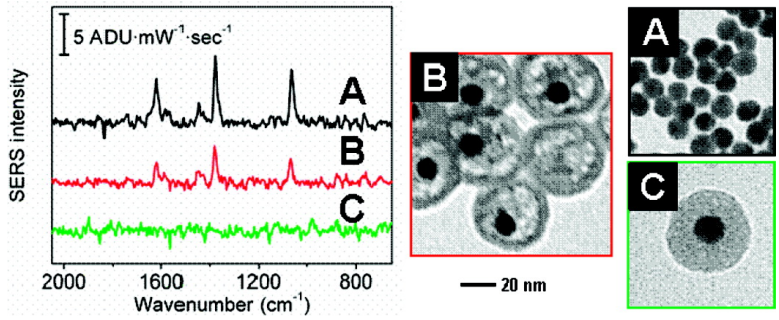

More About This Article

Additional resources and features associated with this article are available within the HTML version:

- Supporting Information
- Access to high resolution figures
- Links to articles and content related to this article
- Copyright permission to reproduce figures and/or text from this article

View the Full Text HTML

Journal of the American Chemical Society is published by the American Chemical Society. 1155 Sixteenth Street N.W., Washington, DC 20036

J|A|C|S
ARTICLES

Published on Web 10/03/2008

Silica−Void−Gold Nanoparticles: Temporally Stable Surface-Enhanced Raman Scattering Substrates

Maryuri Roca and Amanda J. Haes*

Department of Chemistry, University of Iowa, Iowa City, Iowa 52242

Received July 28, 2008; E-mail: amanda-haes@uiowa.edu

Abstract: Reproducible detection of a target molecule is demonstrated using temporally stable solution-phase silica−void−gold nanoparticles and surface-enhanced Raman scattering (SERS). These composite nanostructures are homogeneous (diameter = 45 ± 4 nm) and entrap single 13 nm gold nanoparticle cores inside porous silica membranes which prevent electromagnetic coupling and aggregation between adjacent nanoparticles. The optical properties of the gold nanoparticle cores and structural changes of the composite nanostructures are characterized using extinction spectroscopy and transmission electron microscopy, respectively, and both techniques are used to monitor the formation of the silica membrane. The resulting nanostructures exhibit temporally stable optical properties in the presence of salt and 2-naphthalenethiol. Similar SERS spectral features are observed when 2-naphthalenethiol is incubated with both bare and membrane-encapsulated gold nanoparticles. Disappearance of the S−H Raman vibrational band centered at 2566 cm^{-1} with the composite nanoparticles indicates that the target molecule is binding directly to the metal surface. Furthermore, these nanostructures exhibit reproducible SERS signals for at least a 2 h period. This first demonstration of utilizing solution-phase silica−void−gold nanoparticles as reproducible SERS substrates will allow for future fundamental studies in understanding the mechanisms of SERS using solution-phase nanostructures as well as for applications that involve the direct and reproducible detection of biological and environmental molecules.

Introduction

Since its discovery over 30 years ago, surface-enhanced Raman scattering (SERS) has become a valuable but limited spectroscopic technique for the sensitive detection of molecules.[1,2] Similar to normal Raman spectroscopy, SERS provides both chemical identification and structural information of a molecule based on its unique vibrational fingerprint. Although Raman spectroscopy provides highly specific information regarding a molecule, its use is limited because of inherently low signal intensities and small molecular cross sections versus other spectroscopic techniques.[3] In comparison to normal Raman scattering, SERS has been shown to increase the magnitude of the Raman effect for a given analyte by up to 10^6 to 10^{14} orders of magnitude[1,2,4] and has contributions from both chemical and electromagnetic enhancement effects.[5−7]

Control over the composition, shape, size, and local environment surrounding the metallic substrate is vital for achieving consistent SERS enhancements. In the past 15 years, much progress has been made in controlling these properties via both fabrication[2,8] and synthetic[9−12] techniques. The simplicity of nanoparticles synthesized by metal salt reduction techniques has warranted their widespread use in SERS detection; however, the high surface energy and resulting instability of these materials in solution is often translated into irreproducible SERS signals.[13]

Inconsistencies in these solution-phase measurements have been attributed to changes in the electromagnetic or localized surface plasmon resonance (LSPR) properties of the nanoparticles.[14] Slight variations in either the shape or size of a nanostructure will greatly influence the LSPR of the nanoparticles and, as a consequence, their SERS enhancements. Furthermore, when nanoparticles aggregate, the LSPR of the structures will couple resulting in a new, lower energy extinction band which will impact the intensity of a SERS signal.

To both maintain consistent electromagnetic properties and prevent aggregation, metal nanoparticles have been protected with stabilizing molecules. For instance, nanoparticles can be modified with capping molecules which increase electrostatic

(1) Jeanmaire, D. L.; Van Duyne, R. P. *J. Electroanal. Chem. Interfacial Electrochem.* **1977**, *84* (1), 1–20.
(2) Haes, A. J.; Haynes, C. L.; McFarland, A. D.; Schatz, G. C.; Van Duyne, R. P.; Zou, S. *MRS Bull.* **2005**, *30* (5), 368–375.
(3) Le Ru, E. C.; Blackie, E.; Meyer, M.; Etchegoin, P. G. *J. Phys. Chem. C* **2007**, *111* (37), 13794–13803.
(4) Nie, S.; Emory, S. R. *Science* **1997**, *275* (5303), 1102–1106.
(5) Campion, A.; Kambhampati, P. *Chem. Soc. Rev.* **1998**, *27* (4), 241–250.
(6) Otto, A. *J. Raman Spectrosc.* **1991**, *22* (12), 743–752.
(7) Schatz, G. C.; Young, M. A.; Van Duyne, R. P. *Top. Appl. Phys.* **2006**, *103*, 19–46.
(8) Haynes, C. L.; Haes, A. J.; McFarland, A. D.; Van Duyne, R. P. *Top. Fluoresc. Spectrosc.* **2005**, *8*, 47–99.
(9) Nehl, C. L.; Liao, H.; Hafner, J. H. *Nano Lett.* **2006**, *6* (4), 683–688.
(10) Doering, W. E.; Piotti, M. E.; Natan, M. J.; Freeman, R. G. *Adv. Mater.* **2007**, *19* (20), 3100–3108.
(11) Lal, S.; Grady, N. K.; Kundu, J.; Levin, C. S.; Lassiter, J. B.; Halas, N. J. *Chem. Soc. Rev.* **2008**, *37* (5), 898–911.
(12) Le, F.; Brandl, D. W.; Urzhumov, Y. A.; Wang, H.; Kundu, J.; Halas, N. J.; Aizpurua, J.; Nordlander, P. *ACS Nano* **2008**, *2* (4), 707–718.
(13) Rodger, C.; Rutherford, V.; White, P. C.; Smith, W. E. *J. Raman Spectrosc.* **1998**, *29* (7), 601–606.
(14) Haes, A. J.; Stuart, D. A.; Nie, S.; Van Duyne, R. P. *J. Fluoresc.* **2004**, *14* (4), 355–367.

repulsive forces between nanoparticles and prevent aggregation.[15] An additional advantage of using surface ligands to improve the stability of nanoparticles is that this surface chemistry can be selectively displaced by the target molecule which improves its detectability with SERS; however, these capping molecules can experience chemical degradation, reaction with the metal, or be affected by environmental changes (pH, temperature, ionic strength, etc.).[16] Furthermore, when the surface ligand is displaced or degraded, the nanoparticles often aggregate and cause large changes in the LSPR of the nanoparticles which can either improve or degrade the SERS signal.

The robustness of nanoparticles to chemical and environmental changes has been greatly improved by encapsulating the metal nanoparticle cores in microporous silica shells.[17] Alternatively, composite nanoparticle structures with polymer shell−void−noble metal core architectures have been synthesized[18] and recently used as catalysts.[19] In particular, the use of silica shells offers many advantages including (1) reduction of electromagnetic coupling between metal nanoparticle cores, (2) optical transparency, (3) tunability in the optical properties of metal nanoparticles,[20] (4) versatility in the design of diverse surface morphologies and functionalizations,[21] and (5) improved biocompatibility via surface modification.[22]

Despite these advantages, the use of silica-coated nanoparticles in SERS applications has been limited to the employment of reporter or tag molecules that have been entrapped between the metal core and the silica shell during synthesis.[23−25] Alternatively, silica has been used to eliminate SERS enhancements by purposefully blocking the metal substrate to prevent direct interactions between the molecule and metal.[26] Because silica is composed of a disordered, microporous structure, the diffusion of molecules toward the metal core is limited. Consequently, only slow, inward diffusion of small ions has been reported with these core shell nanostructures.[27]

In this work, we demonstrate the encapsulation of gold nanoparticle cores in porous silica membranes for reproducible and temporally consistent SERS detection. First, silica shells that entrap gold nanoparticle cores will be formed. Next, the less dense and cross-linked internal silica matrix will be selectively etched versus the highly cross-linked external silica membrane. These internally etched silica membranes which contain gold nanoparticle cores (IE Au@SiO_2) will be demonstrated to be viable SERS substrates for the reproducible detection of 2-naphthalenethiol. This work presents the first report of reproducible SERS detection using solution-phase silica−void−gold nanoparticles. These composite nanostructures should allow for fundamental studies in understanding the mechanisms of SERS using solution-phase nanostructures as well as for applications that involve the direct and reproducible detection of biological and environmental molecules.

Experimental Section

Reagents and Chemicals. Amberlite MB-150 mixed bed exchange resin, citric acid, gold(III) chloride trihydrate, (3-aminopropyl)trimethoxysilane (APS), sodium chloride (NaCl), sodium citrate dehydrate, sodium trisilicate (27%), 2-naphthalenethiol (2-NT), and tetraethyl orthosilicate (TEOS) were purchased from Sigma (St. Louis, MO). Ammonium hydroxide, ethanol, hydrochloric acid (HCl), methanol, and nitric acid, were purchased from Fisher Scientific (Pittsburgh, PA). Ultrapure water (18.2 MΩ cm^{-1}) was obtained using a Nanopure System from Barnstead (Dubuque, IA). For all experiments, glassware was cleaned with aqua regia (3:1 HCl/HNO_3), rinsed thoroughly with ultrapure water, and oven-dried overnight before use.

Gold Nanoparticle Synthesis. Gold nanoparticles were synthesized via citrate reduction.[28] Briefly, 50 mL of 1 mM gold(III) chloride trihydrate solution was refluxed and vigorously stirred for 10 min. Once a rolling boil was achieved, 5 mL of 39 mM citrate solution was quickly added, and the solution changed from pale yellow to deep red within 1 min. The solution was refluxed for an additional 10 min and allowed to equilibrate to room temperature while stirring. The resulting gold nanoparticles have a diameter of $d = 13.3 \pm 0.6$ nm, as determined from transmission electron microscopy, and an extinction maximum of $\lambda_{max} = 520$ nm. The nanoparticle concentration was calculated to be 13 nM using the approached reported by Haiss et al.[29]

Synthesis of Microporous Silica-Coated Gold Nanoparticles (Au@SiO_2). Au@SiO_2 nanoparticles were synthesized by combining two methods reported by Liz-Marzan and coworkers.[20,30] Briefly, 40 mL of the gold nanoparticle stock solution was diluted with 40 mL of water and mixed with Amberlite resin to reduce the ionic strength of the solution. The resin was then removed, and the pH of the nanoparticle solution was adjusted to 5.0 using 1 M HCl. Next, the nanoparticles were made vitreophilic via the addition of 1 mM APS (0.52 mL). After 15 min, 27% silicate (60 μL) was added to the solution, and the mixture was stirred for 24 h. The addition of 352 mL of ethanol (to a final ratio of 1:4.4 water/ethanol) induced the precipitation of unreacted silicate. After 6 h, the silica shells were thickened by adding concentrated ammonium hydroxide (0.2 mL), TEOS (20 μL), and 1 mM APS (20 μL). After 16 h, the reaction was stopped and the ethanol removed from the mixture by centrifugation (30 min, 10 000 rpm).

Synthesis of Internally Etched Silica-Coated Gold Nanoparticles (IE Au@SiO_2). IE Au@SiO_2 nanoparticles were synthesized by increasing the pH of the Au@SiO_2 solution. First, the pH of a Au@SiO_2 solution (stirring) was increased via the addition of ammonium hydroxide (1.5 M final concentration). The etching process was quenched with concentrated HCl until the overall solution pH approached ~2.

Nanoparticle Purification. In all composite nanoparticle solutions, careful steps were taken to remove uncoated or partially silica-coated nanoparticles from the Au@SiO_2 or IE Au@SiO_2 nanoparticle solutions which were purified using size exclusion chromatography.

(15) Hunter, R. J. *Introduction to Modern Colloid Science*; Oxford University Press: Oxford, England, 1993.
(16) Neouze, M. A.; Schubert, U. *Monatsh. Chem.* **2008**, *139* (3), 183–195.
(17) LizMarzan, L. M.; Giersig, M.; Mulvaney, P. *Chem. Commun.* **1996**, (6), 731–732.
(18) Kim, M.; Sohn, K.; Na, H. B.; Hyeon, T. *Nano Lett.* **2002**, *2* (12), 1383–1387.
(19) Liu, G. Y.; Ji, H. F.; Yang, X. L.; Wang, Y. M. *Langmuir* **2008**, *24*, 1019–1025.
(20) LizMarzan, L. M.; Giersig, M.; Mulvaney, P. *Langmuir* **1996**, *12* (18), 4329–4335.
(21) Brinker, C. J.; Scherer, G. W. *Sol−Gel Science: The Physics and Chemistry of Sol−Gel Processing*; Harcourt Brace Jovanovich: Boston, MA, 1990.
(22) Gupta, R.; Chaudhury, N. K. *Biosens. Bioelectron.* **2007**, *22* (11), 2387–2399.
(23) Mulvaney, S. P.; Musick, M. D.; Keating, C. D.; Natan, M. J. *Langmuir* **2003**, *19* (11), 4784–4790.
(24) Gong, J. L.; Jiang, J. H.; Yang, H. F.; Shen, G. L.; Yu, R. Q.; Ozaki, Y. *Anal. Chim. Acta* **2006**, *564* (2), 151–157.
(25) Doering, W. E.; Nie, S. *Anal. Chem.* **2003**, *75* (22), 6171–6176.
(26) Olson, L. G.; Lo, Y. S.; Beebe, T. P.; Harris, J. M. *Anal. Chem.* **2001**, *73* (17), 4268–4276.
(27) Ung, T.; Liz-Marzan, L. M.; Mulvaney, P. *Langmuir* **1998**, *14* (14), 3740–3748.
(28) Grabar, K. C.; Freeman, R. G.; Hommer, M. B.; Natan, M. J. *Anal. Chem.* **1995**, *67* (4), 735–743.
(29) Haiss, W.; Thanh, N. T. K.; Aveyard, J.; Fernig, D. G. *Anal. Chem.* **2007**, *79* (11), 4215–4221.
(30) Grzelczak, M.; Correa-Duarte, M. A.; Liz-Marzan, L. M. *Small* **2006**, *2* (10), 1174–1177.

Scheme 1. Encapsulation of Gold Nanoparticle Cores in Microporous Silica Membranes

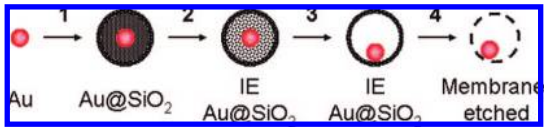

These nanoparticles were purified using a Sephadex-25 column where the bare or partially coated gold nanoparticles were retained while the $Au@SiO_2$ or IE $Au@SiO_2$ nanoparticles were eluted and redispersed in water. The concentration of the $Au@SiO_2$ and IE $Au@SiO_2$ nanoparticle solutions were estimated via extinction spectroscopy and assumed to have an extinction coefficient of 13 nm bare gold nanoparticles ($\varepsilon_{520nm} = 2 \times 10^8\ M^{-1}\cdot cm^{-1}$).

Transmission Electron Microscopy (TEM). TEM was performed using a JEOL JEM-1230 microscope equipped with a Gatan CCD camera. Samples were prepared on 400 mesh copper grids coated with a thin film of Formvar and carbon. The nanoparticle solution was diluted in a 50% water−ethanol mixture. Approximately 50 μL of this solution was pipetted onto a grid and promptly drained using filter paper. The grids were allowed to thoroughly dry before imaging.

Extinction Spectroscopy. Extinction spectra were collected using a UV−vis spectrometer (Ocean Optics HR4000) configured in a transmission geometry. Disposable methacrylate cuvettes (path length = 1 cm) were used. All measurements were taken using the following parameters: 30 ms integration time, average of 30 scans, and boxcar of 10. For continuous spectral acquisition, spectra were recorded every 2 s.

SERS. All SERS spectra were collected using an Advantage200A Raman system (DeltaNu). All measurements were taken using the following parameters: excitation wavelength, $\lambda_{ex} = 633$ nm, integration time = 50 s, power = 2 mW. All spectra were background-corrected using Excel. Spectral intensities were normalized to units of $ADU\cdot mW^{-1}\cdot s^{-1}$. Enhancement factors (EF) were calculated versus a normal Raman spectrum of 8 mM 2-NT in ethanol.

Results and Discussion

Engineering and Characterization of IE $Au@SiO_2$ Nanoparticles. The stepwise synthesis of IE $Au@SiO_2$ nanoparticles is depicted in Scheme 1. First, gold nanoparticles are coated in a composite silica shell. Solid silica shells are prepared via a modified Stöber method[31] in a two-step process whereby a vitreophilic layer which consists of APS and silicate is initially formed on the gold surface. The resulting thin silica layer is required to minimize nanoparticle aggregation and to protect the nanoparticle cores from degradation in subsequent steps. Next, the initial silica layer is thickened using an ethanolic mixture of APS, TEOS, and ammonium hydroxide. Finally, conversion of the silica shell into a silica membrane (i.e., silica−void−gold structure) occurs in an aqueous solution of ammonium hydroxide. The porosity of the resulting IE $Au@SiO_2$ nanoparticles is dictated by the concentration of ammonium hydroxide and etching time. At short times (0−10 min), the resulting nanoparticles are gold nanoparticle cores entrapped in porous silica membranes (2). By extending the etching time, $Au@SiO_2$ nanoparticles with freely moving gold cores (3) and membrane-etched (4) or completely dissolved silica membranes are formed.

In Figure 1, representative TEM images that depict the formation of bare gold (Figure 1A), $Au@SiO_2$ (Figure 1B), as well as IE $Au@SiO_2$ nanoparticles after 10 (Figure 1C) and 15 (Figure 1D) min etching periods are included. As shown in Figure 1B, silica nanoparticles with and without gold cores are formed in this process. Next, the internal silica matrix is slowly etched under basic conditions. Two important observations are noted during this process. First, the silica etching process does not depend on the presence of the gold core. As visible in Figure 1C, all nanoparticles have been internally etched including those that likely contained no original gold core. Second, the diameter of the composite nanoparticle structures remains constant (~45 nm) before and after etching. This indicates that the etching process is occurring primarily at the inner silica matrix. As etching time increases, the internal silica matrix is sufficiently etched allowing the gold core to freely move within the silica membrane. Subsequently, the silica membrane becomes thinner and eventually exposes the gold core.

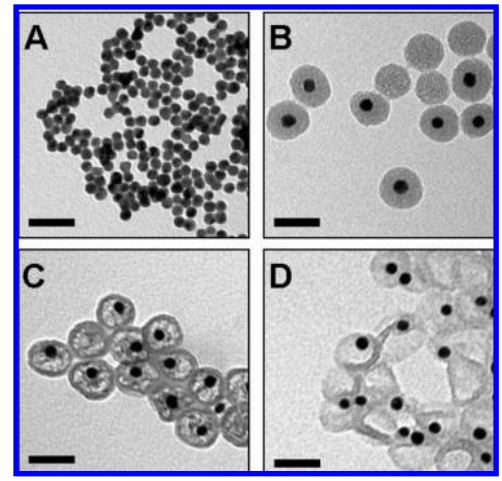

Figure 1. Synthesis of IE $Au@SiO_2$ nanoparticles as revealed in representative TEM images: (A) Au nanoparticles ($d = 13.3 \pm 0.6$ nm), (B) $Au@SiO_2$ nanoparticles ($d = 45 \pm 5$ nm), (C) optimized IE $Au@SiO_2$ nanoparticles (10 min etching time) ($d = 45 \pm 4$ nm), and (D) IE $Au@SiO_2$ (15 min etching time). The scale bar represents 50 nm in all micrographs.

The formation and subsequent dissolution of the silica membrane on $Au@SiO_2$ nanoparticles has also been monitored using extinction spectroscopy (Figure 2). It is well-established that noble metal nanoparticles exhibit a strong extinction (absorption + scattering) band that can be tuned throughout visible to near-infrared wavelengths.[2] This extinction band results when the incident photon frequency is in resonance with the collective oscillation of the conduction band electrons and is known as the LSPR.[2]

In these studies, LSPR spectroscopy has been used to understand the formation and subsequent dissolution of the silica membrane on gold nanoparticles. The optical properties of these composite structures reveal both dielectric changes near the gold nanoparticle cores and electromagnetic coupling between nanoparticles when the silica membrane becomes sufficiently thin. It should be noted that when the electromagnetic fields from two different nanoparticles interact, a complex, lower energy LSPR is produced.[32] As shown in Figure 2A, $Au@SiO_2$ nanoparticles exhibit a single LSPR band centered at 525 nm. Initial formation of the silica *membrane* via dissolution of the silica *shell* is apparent from the initial drop in the extinction intensity and background of this LSPR band (<30 min). As

(31) Stöber, W.; Fink, A.; Bohn, E. *J. Colloid Interface Sci.* **1968**, *26* (1), 62–9.

(32) Ghosh, S.; Pal, T. *Chem. Rev.* **2007**, *107* (11), 4797–4862.

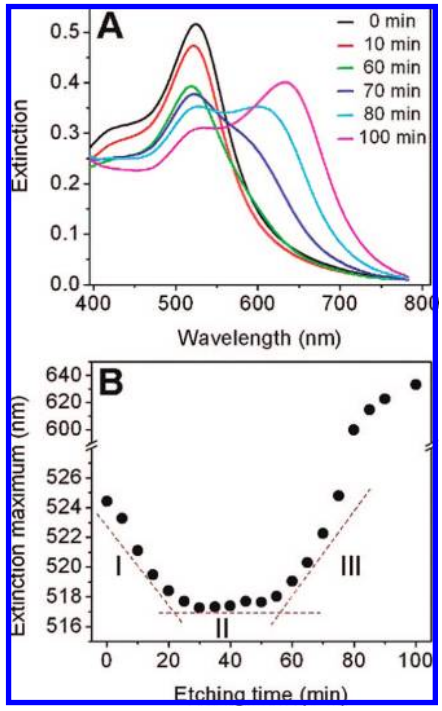

Figure 2. Monitoring the etching process for IE Au@SiO_2 nanoparticles using extinction spectroscopy. (A) Extinction spectra are collected over a 2 h period. (B) The formation of the silica membrane occurs in three distinct stages. Phase I: etching the internal silica matrix. Phase II: dissolution of the remote areas of the membrane vs the metal core. Phase III: complete membrane dissolution. A dashed line has been added to guide the eye.

etching continues, a new extinction band grows in at longer wavelengths (~620 nm). This new LSPR band is characteristic of uncontrollably aggregated or electromagnetically coupled nanoparticles. Comparison of these extinction data to structural characterization with TEM suggests that the silica shell has been sufficiently thinned or fully etched thereby facilitating electromagnetic coupling between multiple nanoparticle cores.

Upon analyzing these data more precisely, three distinct phases in the etching process are clearly observed (Figure 2B). In the first etching phase (phase I), a blue-shift in the extinction maxima of the IE Au@SiO_2 nanoparticles is observed. This decrease in wavelength indicates that the local dielectric environment surrounding the nanoparticles is decreasing and is consistent with silica being replaced by a lower dielectric constant material (water).[2,33] Representative TEM images of these nanoparticles after 10 min of etching (Figure 1C) support this observation and clearly show both a complete outer silica membrane and a less dense internal silica matrix. The progressive blue-shift in the LSPR of the gold nanoparticle cores with increasing etching time indicates the continuous etching of the inner silica matrix. Throughout this phase, both optical and structural characterization support that the external silica shell remains intact. However, as initially revealed in Figure 1D, at the end of phase I (~15 min), the gold nanoparticle cores do not remain in the center of the silica membranes indicating that the inner silica matrix closest to the core is fully etched. Interestingly, at the end of phase I/beginning of phase II, the extinction maxima of the IE Au@SiO_2 nanoparticles stabilize.

During the second phase of the etching process, silica is hypothesized to undergo continual etching at the internal surface of the silica membrane; however, this process occurs beyond the distance dependence of the nanoparticle to dielectric constant variations, and no change in the extinction spectra of the nanoparticles is observed.

After an ~50 min etching period, the optical properties of the nanoparticles begin shifting to longer wavelengths. This final phase of the etching process indicates that the nanoparticles are electromagnetically coupling and that the silica membrane has been breached. Ultimately, dissolution of the silica membrane results in gold nanoparticles with optical properties consistent with uncontrolled aggregation.

Understanding Silica Membrane Formation. The dissolution of the inner silica matrix is clearly observed in Figures 1 and 2. Furthermore, TEM studies reveal that the external silica surface is not etched during this process. In previous studies, similar silica membrane formation was observed for silica-coated carbon nanotubes CNT@SiO_2.[30] This dissolution began at the surface of the CNT and extended radially inward forming an internal void volume with a constant external shell diameter. In contrast, the present IE Au@SiO_2 dissolution studies reveal no radially forming internal void volume but a decrease in the density of the inner silica matrix in smaller domains followed by the dissolution of the outer silica membrane.

These IE Au@SiO_2 nanoparticle data suggest that two distinct silica matrixes (inner and outer) are formed on the surface of the gold nanoparticle cores. As discussed in the synthesis of the (unetched) Au@SiO_2 nanoparticles, both APS and TEOS were used during the formation of the silica shell. As a result, two hydrolysis and condensation reactions will occur to form the composite Au@SiO_2 nanoparticle structure. The following reactions

$$(CH_3-O)_3-Si-(CH_2)_3-NH_2+OH^- \xrightarrow{\text{hydrolysis}} (CH_3-O)_2-Si-(O^-)-(CH_2)_3NH_2+CH_3-OH \quad (1)$$

and

$$(CH_3CH_2-O)_4-Si+OH^- \xrightarrow{\text{hydrolysis}} (CH_3CH_2-O)_3-Si-O^-+CH_3CH_2-OH \quad (2)$$

represent the hydrolysis reactions for APS and TEOS, respectively. Silicate ions formed from TEOS (reaction 2) are less acidic than those produced from APS (reaction 1); however, in both cases, subsequent condensation/precipitation will occur as follows:[21]

$$R_3-SiO^-+\text{cluster}-Si-OH \xrightarrow{\text{condensation}} \text{cluster}-Si-O-Si-R_3 \quad (3)$$

where R = CH_3CH_2−O−, CH_3−O−, or NH_2−$(CH_2)_3$−. As a result, the acidity and relative concentrations of APS and TEOS are hypothesized to drive the formation of the two distinct silica matrixes. Hydrolyzed APS is more acidic and lower in concentration than the hydrolyzed TEOS in the silica matrix. Consequently, APS should be consumed before TEOS in reaction 3. Because silicate bonds that have been formed from APS are less cross-linked than silicate bonds formed from TEOS, the APS-rich inner matrix will be more porous and have a lower density than the external membrane.[34]

(33) Kreibig, U.; Vollmer, M. *Cluster Materials*; Springer-Verlag: Heidelberg, Germany, 1995.

When the silica shell is etched (or silica membrane is formed), reaction 3 will reverse as follows:

$$\text{cluster} - \text{Si} - \text{O} - \text{Si} - \text{R}_3 + \text{OH}^- \xrightarrow{\text{dissolution}}$$

$$\text{R}_3 - \text{SiO}^- + \text{cluster} - \text{Si} - \text{OH} \quad (4)$$

and as a result, dissolution of silica will occur. The more porous and less dense APS-containing matrix will react faster than the denser and highly cross-linked external membrane. This dissolution mechanism is consistent with the observations of silica membrane formation that results in silica−void−gold nanostructures as observed in Figure 1. More complete investigations of the silica shell dissolution mechanism are currently underway.

Assessing the Optical Stability of IE Au@SiO$_2$ Nanoparticles. As mentioned previously, the optical properties of noble metal nanoparticles exhibit unique extinction spectra which arise from their LSPR, a phenomenon not observed in bulk materials.[7,35−37] The local electromagnetic fields accompanying excitation of the LSPR is a key factor in the intense signals observed in all surface-enhanced spectroscopies, including SERS.[2,38] One limitation of using standard solution-phase noble metal nanoparticles for surface-enhanced spectroscopic experiments is the instability of these nanostructures in the presence of target molecules. As a result, nanoparticle optical properties can vary significantly which influences their electromagnetic properties and prevents quantitative detection of target molecules.

The optical stability of citrate-reduced gold and IE Au@SiO$_2$ nanoparticles in the presence of salt are compared in Figure 3. As expected, the optical stability of bare gold nanoparticles is disrupted by the addition of NaCl (Figure 3A). When salt is added to the solution, the electrostatic repulsive forces induced by the citrate ions at the surface of the nanoparticles are diminished in the presence of salt ions, and consequently, the nanoparticles aggregate. When this occurs, the LSPR of the nanoparticles couple and a new, lower energy extinction band centered at ~650 nm is detected.

In contrast, IE Au@SiO$_2$ nanoparticles are optically stable and have an extinction band centered at ~520 nm which is conserved in the presence of salt (Figure 3B). The silica membrane physically impedes electromagnetic coupling between the metal cores. Furthermore, the LSPR of IE Au@SiO$_2$ nanoparticles is similar to that of bare gold nanoparticles (at $t = 0$) and Au@SiO$_2$ nanoparticles, that is, they agree within a few nanometers of each other (Au@SiO$_2$ data not shown). Clearly, silica membranes conserve the optical properties of the gold nanoparticle cores in harsh environments without significantly altering their optical properties versus bare gold nanoparticles.

SERS Activity of Bare and Composite Nanoparticles. To assess how the optical properties of nanoparticles influence

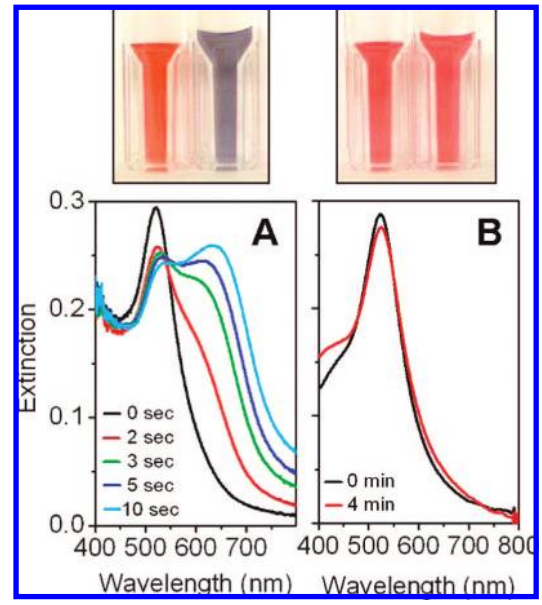

Figure 3. Assessing the optical stability of bare and IE Au@SiO$_2$ nanoparticles in the absence and presence of 0.1 M NaCl. (A) When bare gold nanoparticles are exposed to NaCl, the LSPR centered at 520 nm decreases in intensity while a new band forms at longer wavelengths. (B) IE Au@SiO$_2$ nanoparticles are stable in the presence of NaCl. Digital photographs of the nanoparticle solutions are included above the respective extinction spectra. Photographs at $t = 0$ (left) and $t = 10$ s (right) for uncoated gold nanoparticles and $t = 0$ (left) and $t = 4$ min (right) are included for IE Au@SiO$_2$ nanoparticles.

resulting SERS signals, gold, Au@SiO$_2$, and IE Au@SiO$_2$ nanoparticles have been incubated with 2-NT. This molecule was chosen for several reasons. First, 2-NT has a high affinity for the gold core. Second, the molecular size of 2-NT permits its diffusion through the microporous silica membrane which has an estimated pore size of ~15 Å.[34] Finally, the molecule has a large Raman cross section and is moderately soluble in water.

In preliminary experiments, the concentrations of both nanoparticles and 2-NT were optimized to minimize bare gold nanoparticle aggregation. Under these optimized conditions, bare gold nanoparticles exhibit large SERS signals (Figure 4A-1); however, these signals vary drastically with time and from run to run. After a silica shell is grown on these structures (Figure 4A-3), no SERS signal is observed regardless of 2-NT concentration and incubation time. Au@SiO$_2$ nanoparticles exhibit no SERS activity because the molecule is not able to interact with the metal core surface required for satisfying the chemical enhancement and/or the silica shell extends beyond the strong electromagnetic fields near the gold surface, an interaction required for electromagnetic enhancement.

As shown in Figure 4A-2, IE Au@SiO$_2$ nanoparticles exhibit SERS enhancement for 2-NT. To understand this spectroscopic response, we must understand the role of both the thickness and porosity of the silica membrane on the IE Au@SiO$_2$ nanoparticles. We hypothesize that the observed SERS response is from molecules that have diffused inside the silica membrane. This is based on three experimental observations. First, the SERS signal is not detected immediately after the molecule is added to the nanoparticle solution. Instead, more than 1 min is required before a SERS signal is detected, thereby indicating that the molecule needs time to diffuse through the silica membrane and bind to the gold nanoparticle core. Second, the silica membrane has an estimated thickness of ~3−4 nm (from TEM).

(34) Van Blaaderen, A.; Vrij, A. *J. Colloid Interface Sci.* **1993**, *156* (1), 1–18.
(35) Haynes, C. L.; Van Duyne, R. P. *J. Phys. Chem. B* **2001**, *105* (24), 5599–5611.
(36) Link, S.; El-Sayed, M. A. *J. Phys. Chem. B* **1999**, *103* (40), 8410–8426.
(37) Kreibig, U.; Gartz, M.; Hilger, A.; Hovel, H. Optical Investigations of Surfaces and Interfaces of Metal Clusters. In *Advances in Metal and Semiconductor Clusters*; Duncan, M. A., Ed.; JAI Press Inc.: Stamford, CT, 1998; Vol. 4, pp 345−393.
(38) Schatz, G. C.; Van Duyne, R. P. *Electromagnetic Mechanism of Surface-Enhanced Spectroscopy*; Wiley: New York, 2002; Vol. 1, pp 759−774.

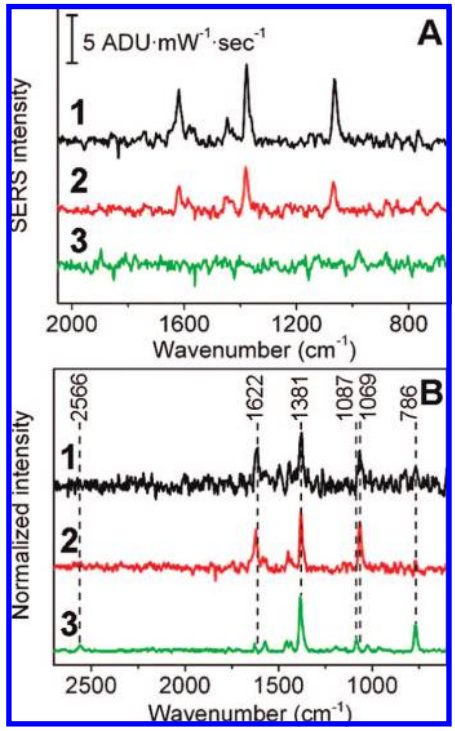

Figure 4. Raman and SERS data for 2-NT. (A) Solution-phase SERS spectra of 4 mM 2-NT with 4 nM (1) bare gold nanoparticles (irreproducible), (2) IE Au@SiO_2, and (3) Au@SiO_2 nanoparticles. Spectral averages of 1, 10, and 6 were used in 1, 2, and 3, respectively. (B) Normalized spectra of 2-NT with (1) IE Au@SiO_2 (SERS), (2) bare gold nanoparticles (SERS), and (3) a supersaturated suspension of 2-NT in water (Raman). The most significant vibrational bands are labeled. Experimental conditions are as follows: λ_{ex} = 633 nm, power = 2.0 mW, SERS integration time = 50 s, Raman integration time = 10 s. Spectral averages of 10, 1, and 10 were used in 1, 2, and 3, respectively.

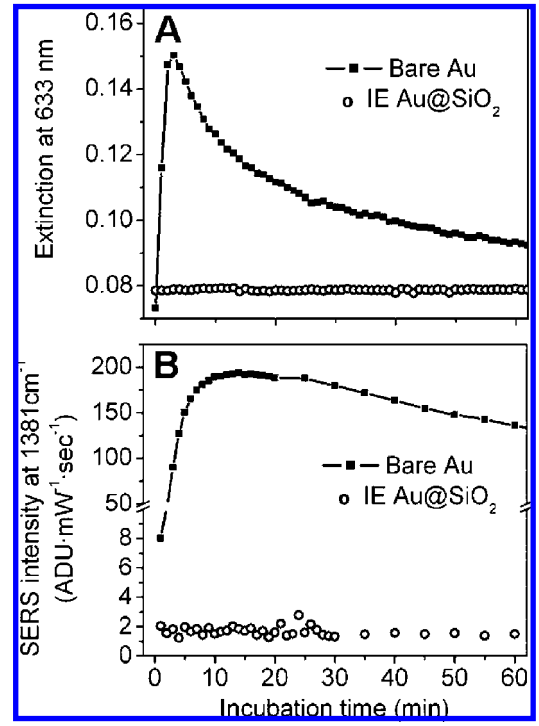

Figure 5. Monitoring the extinction and SERS intensity for nanoparticle samples upon 2-NT addition as a function of time. (A) Real-time changes in the extinction intensity at the Raman excitation wavelength (λ_{ex} = 633 nm) are shown for bare gold and IE Au@SiO_2 nanoparticles. Spectra were collected every 1 min. (B) Real-time behavior of the SERS intensity at 1381 cm^{-1} reveals distinct responses to the nanoparticle samples. λ_{ex} = 633 nm, power = 2.0 mW, integration time = 50 s. In both panels, solid squares = bare gold nanoparticles and open circles = IE Au@SiO_2 nanoparticles. Identical nanoparticle and 2-NT concentrations are used in Figure 4.

Approximately 1 order of magnitude in SERS intensity is lost per nanometer that the target molecule is from the enhancing substrate.[39−41] If the SERS signal observed with IE Au@SiO_2 nanoparticles results from molecules outside the silica membrane, the SERS signals for both the Au@SiO_2 and IE Au@SiO_2 should be identical. Clearly, this is not the case. Instead, these results suggest that 2-NT is able to diffuse through the silica membrane of IE Au@SiO_2 nanoparticles and subsequently bind to the surface of the gold nanoparticle cores.

Finally, the direct adsorption of 2-NT to the gold core in IE Au@SiO_2 nanoparticles is evident by comparing spectral differences between Raman and SERS spectra for 2-NT (Figure 4B). Vibrational band assignments were made according to the literature.[42] In all spectra for 2-NT, vibrational bands at 1381 (strong, ring stretching) and 786 (weak, ring deformation) cm^{-1} are present; however, several spectral differences are also noted. First, a C−H bending mode centered at 1087 cm^{-1} in the normal Raman spectrum shifts to 1069 cm^{-1} in both SERS spectra. Previously, it was reported that 2-NT binds perpendicular to the metal surface thereby preferentially enhancing and shifting the vibration mode at 1069 cm^{-1}.[42] This is observed in the spectral data for both bare gold and IE Au@SiO_2 nanoparticles but not in the Raman spectrum. Additionally, the ring stretching mode centered at 1628 cm^{-1} in the Raman spectrum shifts to 1622 cm^{-1} in the SERS spectra. Finally, the S−H stretch at 2566 cm^{-1} is only present in the Raman spectra suggesting that this bond is no longer present in the IE Au@SiO_2 nanoparticle studies and that a chemical bond has formed between the gold surface and sulfur group. These spectral changes further support the hypothesis that 2-NT is binding directly to the gold surface in the IE Au@SiO_2 nanoparticle structures.

Time-Dependent SERS Studies. When engineering nanoparticles for reproducible SERS detection, it is important to compare the optical properties of the nanoparticles to the observed SERS enhancement at a fixed vibrational frequency over time. Following the addition of 2-NT, the solution was briefly vortexed and spectra were collected every 50 s. The extinction intensity at 633 nm and SERS intensity for the ring stretching mode centered at 1381 cm^{-1} is shown in Figure 5, parts A and B, respectively. As can be seen in Figure 5A, the extinction intensity of bare gold nanoparticles at 633 nm doubles within the first minute of exposure to 2-NT; but after 2 min, this extinction intensity steadily decreases. This response is consistent with nanoparticles that are aggregating and settling out of solution.[43] In contrast, the extinction intensity at 633 nm for IE Au@SiO_2 remains constant after the addition of 2-NT and electromagnetic coupling between the gold cores is prohibited by the silica membrane.

(39) Kennedy, B. J.; Spaeth, S.; Dickey, M.; Carron, K. T. *J. Phys. Chem. B* **1999**, *103*, 3640–3646.
(40) Ye, Q.; Fang, J. X.; Sun, L. *J. Phys. Chem. B* **1997**, *101* (41), 8221–8224.
(41) Tsen, M.; Sun, L. *Anal. Chim. Acta* **1995**, *307* (2−3), 333–340.
(42) Alvarez-Puebla, R. A.; Dos Santos, D. S.; Aroca, R. F. *Analyst* **2004**, *129* (12), 1251–1256.
(43) Tantra, R.; Brown, R. J. C.; Milton, M. J. T. *J. Raman Spectrosc.* **2007**, *38*, 1469–1479.

It is clear that from these data that bare gold and IE Au@SiO_2 nanoparticles exhibit different optical responses when 2-NT is added to the solution as observed in Figure 5A. Next, to compare and quantify SERS signals for the different nanoparticle structures, Raman enhancement factors (EF) were calculated using the following equation:[3]

$$\mathrm{EF} = \frac{I_{\mathrm{SERS}} C_{\mathrm{Raman}}}{I_{\mathrm{Raman}} C_{\mathrm{SERS}}} \quad (5)$$

where C_{Raman} is the concentration of analyte that produces a Raman signal I_{Raman}, and C_{SERS} is the concentration of analyte that produces a SERS signal I_{SERS}.

We should note that the EFs for all SERS measurements have a contribution from both electromagnetic and chemical components.[44] The electromagnetic component relies on the optical properties of the nanoparticles and can contribute up to 10^{12} orders of magnitude in SERS enhancement.[45,46] The chemical enhancement mechanism, on the other hand, is related to the charge transfer as well as a physical interaction between the nanoparticle and target molecule and contributes up to 10^2 orders of magnitude in SERS experiments.[5]

The observed changes in the optical properties of the nanoparticles have large impacts on SERS enhancement of 2-NT. In Figure 5B, two important trends are observed. First, the SERS enhancement for both bare and IE Au@SiO_2 nanoparticles follows the time-dependent extinction data observed in Figure 5A. Because the bare gold nanoparticles have constantly changing optical properties, the observed SERS signals also fluctuate. IE Au@SiO_2 nanoparticles have stable optical properties, and as a result, SERS intensities are also stable and quantitative. Second, the magnitude of the SERS intensity for the bare gold nanoparticles is much larger than the SERS intensity for the IE Au@SiO_2 nanoparticles. This response is expected as the extinction intensity of the IE Au@SiO_2 nanoparticles is much smaller than that for the bare gold nanoparticles at the selected SERS excitation wavelength because no electromagnetic coupling between nanoparticle cores (aggregation) has occurred.

It is important to note that bare nanoparticles exhibit irreproducible SERS enhancements which have been attributed to the aggregation of the nanoparticles upon 2-NT addition. A maximum EF of 4×10^4 is observed for bare gold nanoparticles, whereas an average EF of 3×10^2 is obtained for IE Au@SiO_2 nanoparticles. It should be noted that the average signal strength for bare gold nanoparticles varies by 3000% over a 2 h period. In comparison, both the detector response for normal Raman scattering and SERS signal strength from IE Au@SiO_2 nanoparticles vary by ~10%. This suggests that signal variation from IE Au@SiO_2 nanoparticles arises from fluctuations in the detector response (or laser power)—not from changes in the electromagnetic properties or stability of the nanoparticles! Finally, the extinction intensity for IE Au@SiO_2 nanoparticles is weak at the excitation wavelength. As a result, the magnitude of the SERS enhancement observed for these nanoparticles is small and consistent in magnitude with a dominant chemical enhancement and/or slight electromagnetic enhancement. Further refinement and improvement in the optical properties of the nanoparticle core and structure of the silica membrane will aid in improving the magnitude of this enhancement for IE Au@SiO_2 nanoparticles and understanding molecular diffusion of analytes through the silica membrane, respectively.

Conclusions

This work presents the first report of temporally consistent SERS detection using solution-phase silica−void−gold nanoparticles. Specifically, the principal discovery reported here is that quantitative and temporally stable SERS signals are achieved using solution-phase gold nanoparticle cores that have been entrapped in porous silica membranes. These composite silica−void−gold nanostructures were synthesized in a stepwise process. First, gold nanoparticles were encapsulated in a thin silica matrix formed from APS and TEOS. Next, a denser silica shell composed of TEOS encapsulated the initial silica matrix. Finally, the less cross-linked (APS-containing) silica domains were etched before the dissolution of the outer silica membrane and resulted in microporous silica membranes that both encapsulated and prevented electromagnetic coupling/aggregation between gold nanoparticle cores.

Detection of target species using SERS occurred after the molecules diffused through the silica membrane. The magnitude and reproducibility of the SERS enhancements for 2-NT that was mixed with gold and internally etched Au@SiO_2 nanoparticles were compared. In both cases, the intensity of the SERS signal correlated with changes in the extinction intensity of the nanoparticles at the SERS excitation wavelength. Furthermore, after a brief equilibration period for the diffusion of the molecules into the nanostructure core, the optical properties and SERS enhancements of the target molecule using the internally etched Au@SiO_2 nanoparticles were demonstrated to be constant for at least 2 h. Further refinement of the electromagnetic properties of the gold nanoparticle core should lead to larger SERS enhancements for target molecules. The demonstration of these nanostructures as stable SERS substrates for the quantitative and reproducible detection of a target molecule suggests that these composite structures could be used in a variety of biomedical and environmental applications where sensitive detection is required. Finally, expansion of the presented composite nanostructure synthesis to other core materials has the potential to increase the long-term stability of any nanomaterial where instability and high surface energy might traditionally reduce their usefulness in complex environments.

Acknowledgment. The authors gratefully acknowledge financial support the Department of the Navy, Office of Naval Research (YIP Award No. N00014-07-1-0827), the Society of Analytical Chemists of Pittsburgh, and the University of Iowa. The authors also acknowledge the Central Microscopy Research Facility (CMRF) for use of the TEM.

JA8059039

(44) Moskovits, M. *J. Raman Spectrosc.* **2005**, *36* (6−7), 485–496.
(45) Kneipp, K.; Kneipp, H.; Kneipp, J. *Acc. Chem. Res.* **2006**, *39* (7), 443–450.
(46) McFarland, A. D.; Young, M. A.; Dieringer, J. A.; Van Duyne, R. P. *J. Phys. Chem. B* **2005**, *109* (22), 11279–11285.